

Thermal Conductivity Measurements on Icy Satellite Analogs

Aurya Javeed*
Martin Barmatz,† Fang Zhong,† and Mathieu Choukrount†

Introduction

1.1 Background

With regard to planetary science, NASA aspires to: “Advance scientific knowledge of the origin and history of the solar system, the potential for life elsewhere, and the hazards and resources present as humans explore space” [1].

In pursuit of such an end, the Galileo and Cassini missions garnered spectral data of icy satellite surfaces implicative of the satellites’ structure and material composition. The potential for geophysical modeling afforded by this information, coupled with the plausibility of life on icy satellites, has pushed Jupiter’s Europa along with Saturn’s Enceladus and Titan toward the fore of NASA’s planetary focus.

Understanding the evolution of, and the present processes at work on, the aforementioned satellites falls squarely in-line with NASA’s cited goal.

1.2 Motivation

An understanding of a satellite is, of course, predicated by an understanding of the properties of its constituent components. Consider the tectonic processes fueling a satellite’s geologic development: the heat flows from which they stem are shaped by the thermal conductivity of internal materials.

Therefore, as a means of further constraining the models of our Solar System’s icy satellites, the Applied Low Temperature Physics Group intends to measure the thermal conductivity of suspected icy satellite analogs—i.e., water ice, salt hydrates, and clathrate hydrates—as functions of the analogs’ temperature, stress, and composition.

In order to do so, the unique cryogenic apparatus depicted in Fig. 1 has been developed. The air piston supplies a force, which—in turn—is transmitted to the analog sample via a MACOR rod and quantified by load cell. Any concomitant changes in sample thickness are measured by a linear variable differential transformer (LVDT).

Samples variegated in microstructure will be subjected to compressions of up to 4 MPa and temperatures ranging between 170 and 270 K.

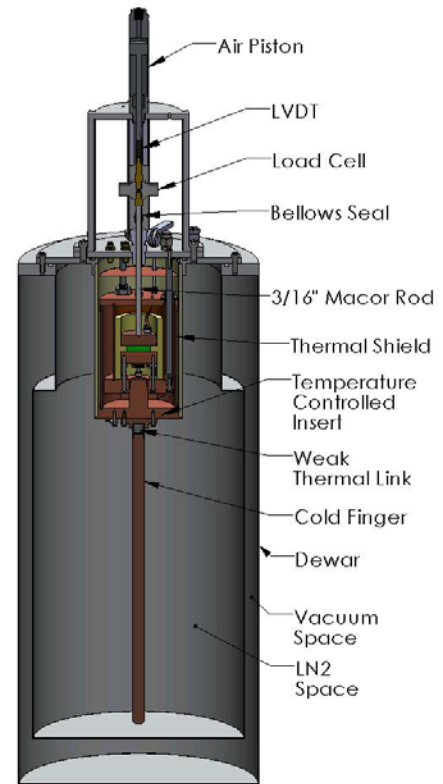


Figure 1: Cryogenic apparatus employed for thermal conductivity measurements.

* The University of Arizona

† Jet Propulsion Laboratory, California Institute of Technology

Objectives

Presented below are the four objectives of my summer internship at JPL.

1. Calibrate the apparatus's thermal conductivity measurement to zeroth order.
2. Calibrate the apparatus's thermal conductivity measurement to first order.
3. Characterizing the apparatus's compliance to stress
4. Manufacture an icy satellite analog and measure its thermal conductivity.

Approach

3.1 Zeroth-Order Conductivity Corrections

Figure 2 depicts the sample housing. Two cylindrical, copper platens sandwich the sample while a temperature-controlled shield maintains a controlled environment.

The zeroth-order data deduction of thermal conductivity assumes one-dimensional, axial heat flow:

A measurement begins with proportional-integral derivative (PID) feedback controls that hold the shield and two platens at constant temperatures. When the top platen's temperature is changed by amount ΔT , the PID control at the bottom platen will attempt to maintain the bottom platen's steady-state temperature by adjusting its heat current by amount $\Delta \dot{Q}$.¹

Enter the axial heat flow assumption: since the temperatures of the bottom platen and the shield remain unchanged, the heat flows from the bottom platen to the shield remain unchanged. Thus the measured change in the PID control heat current $\Delta \dot{Q}$ must come from the top platen and its entirety must traverse the sample. Therefore—if h and A indicate the thickness and cross-sectional area of the sample, respectively—thermal conductivity (λ) should follow from

$$\lambda = -\frac{h\Delta\dot{Q}}{A\Delta T} \quad \text{Equation 1}$$

Of course, things are not so simple. Take note of the position of the heaters and thermometers shown in silver in Fig. 2: even under the assumption of axial heat flow, they

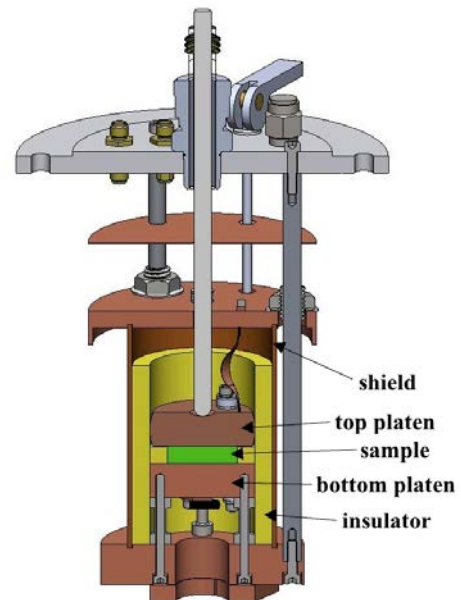


Figure 2: Sample housing detail.

¹ Lest the reader wonder: such an amount is measured directly by the Joule heat change across a 50 ohm precision resistor.

measure not ΔT and $\Delta\dot{Q}$ across the sample, but ΔT and $\Delta\dot{Q}$ of the sample in series with the platens and in parallel with adjacent insulation.

Revisions of Eq. 1 that correct for these—and, more generally, any other—simplifications in the axial heat flow model presented in blocked text are defined as “zeroth-order conductivity corrections”. The phrase follows from Eq. 1’s status as the zeroth-order term in the Taylor expansion of sample conductivity as a function of fundamental observables.

3.1.1 Copper Platen Corrections

As mentioned two paragraphs before: ΔT and $\Delta\dot{Q}$, in actuality, respectively symbolize the temperature and heat current differential across the sample in series with the platens and in parallel with adjacent insulation. Consequently, the measured thermal resistance—defined as

$$R = -\frac{\Delta T}{\Delta\dot{Q}} \quad \text{---} \quad \text{Equation 2}$$

may be decomposed as one would decompose its electrical analog; namely:

$$R = R_{eq} + R_{platens} \quad , \quad \text{Equation 3}$$

where R_{eq} symbolizes the equivalent resistance of the sample and insulator in parallel. Rearranging and employing the definition of thermal resistance reveals

$$\frac{\Delta T}{\Delta\dot{Q}_{eq}} = \frac{\Delta T}{\Delta\dot{Q}} - \frac{\Delta T}{\Delta\dot{Q}_{platens}} \quad . \quad \text{Equation 4}$$

By replacing the sample of Fig. 2 with copper shim stock, same diameter but only 0.005” thick, and removing the adjacent insulation, $\Delta T_{platens}$ and $\Delta\dot{Q}_{platens}$ were measured at 177, 190, and 210 kelvin in accordance with the procedure outlined in blocked text. The shim stock recreated the non-uniform heat flux through the platens present with the sample and adjacent insulation in place.

An interpolation—from the discrete data set—of resistance as a continuous function of temperature was achieved by chi-square minimization. Each of six functional forms of copper resistivity as a function of temperature was scaled by an effective platen geometry fit against the discrete, empirical data. Figure 3 illustrates the optimal fit.

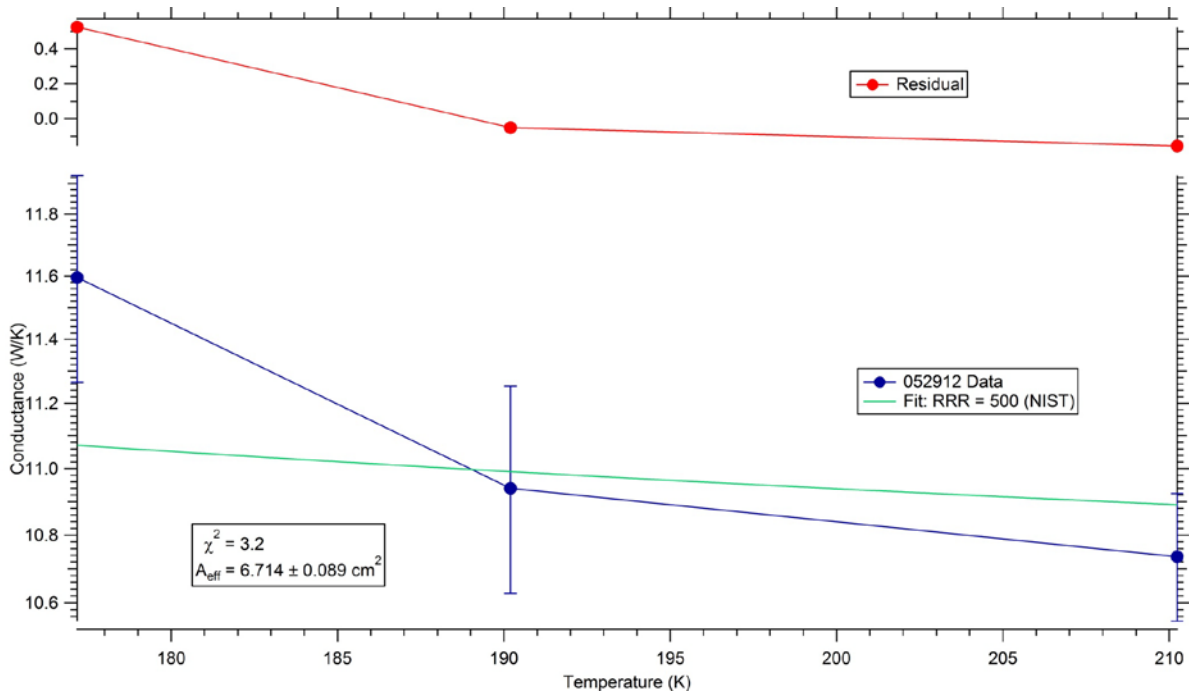


Figure 3: Copper Conductance v Temperature. Overlaid with the empirically derived values (blue) is the lowest chi-square effective geometry fit of the NIST functional forms (green).

The six curves are each specific to a particular residual-resistance ratio (RRR) of copper and published as a standard by the National Institute of Standards and Technology (NIST).

3.1.2 Adjacent Insulation Corrections

Extracting the sample's thermal conductivity from R_{eq} again amounts to analyzing an electrical analog of the thermal path. Because the sample and adjacent insulation are in parallel, their equivalent resistance may be decomposed as

$$\frac{1}{R_{eq}} = \frac{1}{R_{sample}} + \frac{1}{R_{insulator}} \quad \text{--- Equation 5}$$

or, equivalently,

$$\frac{\Delta\dot{Q}}{\Delta T_{sample}} = \frac{\Delta\dot{Q}}{\Delta T_{eq}} - \frac{\Delta\dot{Q}}{\Delta T_{insulator}} \quad \text{Equation 6}$$

after rearranging and employing the definition of thermal resistance.

To quantify the adjacent insulation's conductance as a function of temperature a weighted, second-order polynomial fit was applied to a discrete set of insulator conductivity values published by the manufacturer. Figure 4 illustrates the optimal fit.

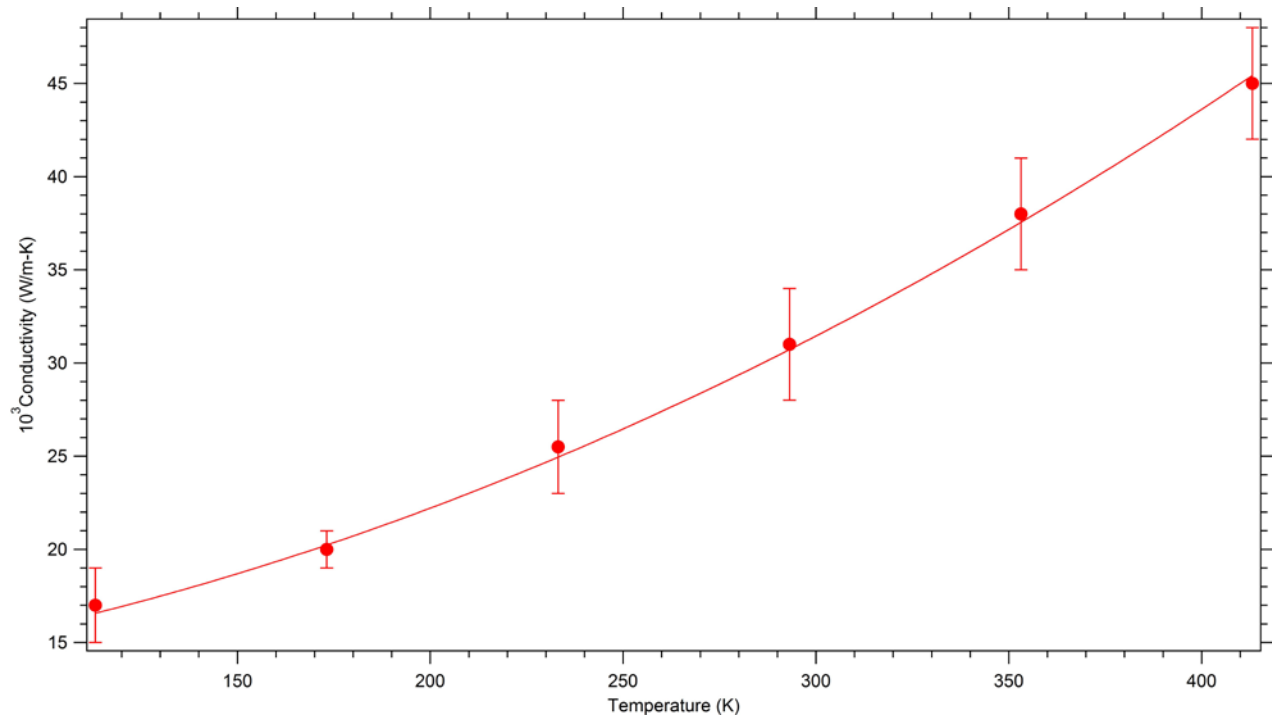


Figure 4: Adjacent Insulation Conductivity v Temperature. Overlaid with the manufacturer's published insulator conductivity values (dots and bars) is a weighted, second-order polynomial fit (line).

Conductance followed from scaling the adjacent insulation's conductivity by its well-defined geometry. ROHACELL[®] is the adjacent insulation's market name.

3.2 First-Order Conductivity Corrections

Recall the Taylor expansion of sample conductivity as a function of fundamental observables mentioned at the bottom of this report's second page. With its zeroth-order term properly accounted for, its first-order term—quantifying transgressions from single-dimensional, axial heat flow—becomes the object of focus.

In the standard, axial-flow thermal conductivity measurement technique, the lateral sides of the platen-sample ensemble would be surrounded by vacuum. Doing so ensures their adiabaticity and validates the single-dimensional, axial heat flow assumption. Unfortunately however, the necessity of maintaining this experiment's samples' saturated vapor pressures precludes a vacuum. The insulation's high thermal resistivity provides ground for assuming axial flow regardless, but such an assumption must be justified through the first-order term mentioned in the preceding paragraph.²

Presently, the validity in using an analogous electrical circuit in modeling the three-dimensional heat flow through the sample housing is being investigated. Figure 5 illustrates a preliminary schematic.

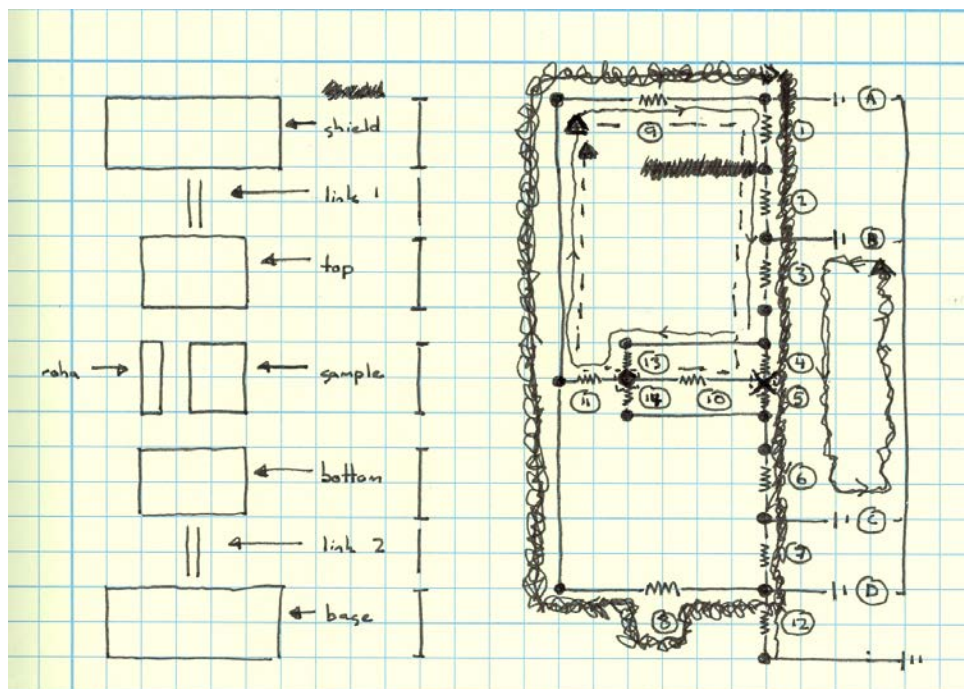


Figure 5: Preliminary schematic of analogous electrical circuit representing three-dimensional heat flow through sample housing. Loops (nodes) signify paths (points) along (upon) which applications of Kirchhoff's laws are of interest.

² One might argue lateral loss may be eliminated by adjusting the shield's temperature to the mean platen temperature. The shield's thermal contact with the rest of the sample housing ensures doing so is never a possibility.

Thermal resistances of the sample housing’s components as functions of temperature are actively being measured by strategically varying temperatures of the sample housing’s platens, base, and shield. Ideally, Kirchhoff’s circuit laws will link these resistances to heat flow through the sample housing.

3.3 Compliance Characterization

The zeroth-order conductivity corrections of §3.1 are founded on the principle of linear superposition: Eq. 4 (6) asserts that the total resistance (conductance) of a thermal path is equivalent to the sum total of the resistances (conductances) of path’s constituent components.

In the same way, the total displacement measured by the LVDT in response to an applied load is equivalent to the sum total of the displacements of the load path’s constituent components. Therefore, it follows that the displacement of the sample in response to an applied load is equivalent to the total displacement measured by the LVDT modulo the rest of the cryogenic apparatus.

A quantification of the response of the cryogenic apparatus without the sample as a function of an applied load is defined as “compliance characterization”. The phrase follows from compliance’s definition as the inverse of stiffness.

Figure 6 illustrates preliminary measurements of the total displacement measured by the LVDT as a function of applied load. A sample of fused quartz was mounted in the apparatus for the measurements.

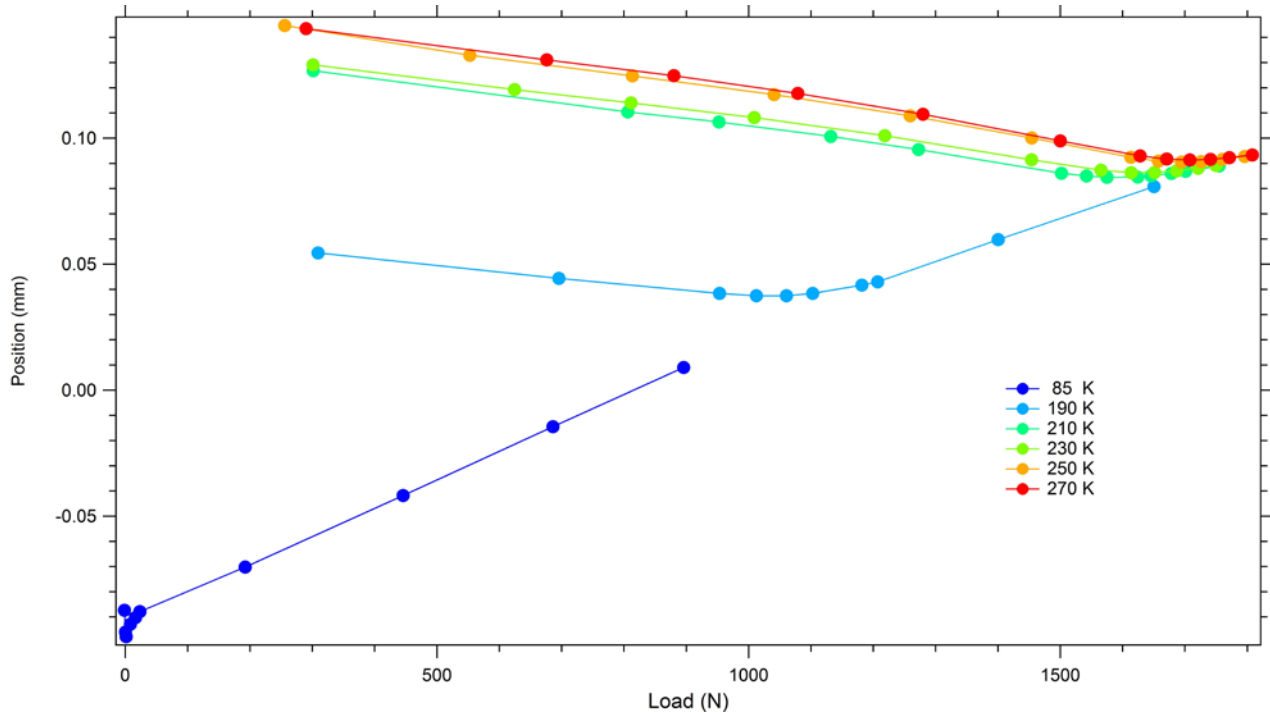


Figure 6: Total Displacement Measured by the LVDT v Applied Load. Measurements were taken at 85, 190, 210, 230, 250, and 270 kelvin. A ¼-inch sample of fused quartz was mounted in the apparatus throughout.

The minima of Fig. 6 were unexpected. Because none of the yield strengths of the load path’s constituent components were exceeded, downward-sloping lines were expected.

In an attempt to isolate the problem, the sample housing and MACOR rod were replaced with a stainless steel plate. The minima were found to stem from the piston's base pushing the LVDT's shell down along with the rod. The problem was remedied by mounting the LVDT's shell slightly closer to the load cell.

3.4 *Analog Preparation*

3.4.1 Press Preparation

Figure 7 shows the primary components of the ice press employed in preparing icy satellite analogs.

Press preparation begins by applying Apiezon N grease to the top and bottom faces of Fig. 7's press body, the interior of the bottom flange, eight screws, and an o-ring.

With the press pieces greased, the press's assembly follows. Figure 7's bottom flange is mounted so that its copper lead is coplanar with the press body's. Four of the eight greased screws are then bolted through the bottom flange, into the press body in order to fix the two together. The o-ring is placed into a corresponding groove cut into the press body's top face for the final assembly step.

The assembled press its components must be cooled below ice's freezing point, but—prior to doing so—the potential for condensation between the press body and bottom flange is limited by applying a cord of weather-proofing tape to the seam between the two. Masking tape is placed atop the weather-proofing tape as a means of holding the latter in position.



Figure 7: Primary components of ice press employed in preparing icy satellite analogs. The press body is sandwiched between top and bottom flanges and adjacent to a hardened, pressing cylinder.

3.4.2 Water Ice Preparation

Figure 8 shows the working area of the cold room in JPL's building 117.



Ice preparation begins by pouring distilled water into a clean plastic bag and allowing it to freeze—see Fig. 8. The solid ice is then shattered, by way of a hammer, into smaller pieces and placed into Fig. 8’s blender to be ground further. Because the heat exuded by the blender’s motor threatens to melt the ice, the blender is run only for approximately one out of every three seconds. The ice puree is stirred with a screwdriver when its loosening is a necessity. After sufficient blending, the puree is poured into Fig. 8’s set of stacked sieves and sieved down to the requisite grain size.

Upon attaining enough grains to fill the ice press up to its top lead, the ice is poured into the prepared press and the top flange is bolted down using the four greased screws remaining from §3.4.1. The hardened cylinder is then placed in after the ice.

3.4.3 Pressing

Figure 9 shows the pressing apparatus—excepting the ice press itself—employed in preparing icy satellite analogs.

Ice pressing begins with placing the ice press in Fig. 9’s metal bucket and connecting the ice press’s leads with the leads of Fig. 9’s vacuum pump. Subsequent to doing so, both the bucket and cold trap are filled with dry ice. The vacuum pump is turned on.

The oil press of Fig. 9 is used to drive the hardened cylinder into the ice. Beginning at 0 pounds per square inch, the pressure on the hardened cylinder is increased by about 200 pounds per square inch every 15 minutes, up to 7000 pounds per square inch.³ Throughout each 15 minute increment, the pressure on the hardened cylinder is held constant by the oil press operator. At 7000 pounds per square inch the oil press operator maintains a constant pressure on hardened cylinder for about 60 minutes.

The pressure on the ice is then decreased by about 100 pounds per square inch every 10 minutes so as not to exceed the tensile strength of ice.



Figure 9: Pressing apparatus—excepting the ice press itself—employed in preparing icy satellite analogs. From top to bottom: oil press, metal bucket, cold trap, and vacuum pump.

³ It may be necessary to insert a spacer between order to drive the hardened cylinder

Upon reaching 0 pounds per square inch, the bottom flange is removed and the ice is pressed out, through the bottom of the ice press.

Results

4.1 Zeroth-Order Conductivity Corrections

Substituting the reciprocal of Eq. 4 into Eq. 6 relates the sample's conductance to the measured resistance explicitly; namely,

$$\frac{\Delta\dot{Q}}{\Delta T_{sample}} = \frac{1}{\Delta T / \Delta\dot{Q} - \Delta T / \Delta\dot{Q}_{platens}} - \frac{\Delta\dot{Q}}{\Delta T_{insulator}} \quad \text{Equation 7}$$

The sample's conductivity follows from replacing Eq. 1's measured conductance with the sample's corrected conductance:

$$\lambda = -\frac{h\Delta\dot{Q}}{A\Delta T_{sample}} \quad \text{Equation 8}$$

Figure 10 illustrates the application of Eq. 7 and 8 to data taken on a fused quartz sample ¼ inch thick and 1 inch in diameter.

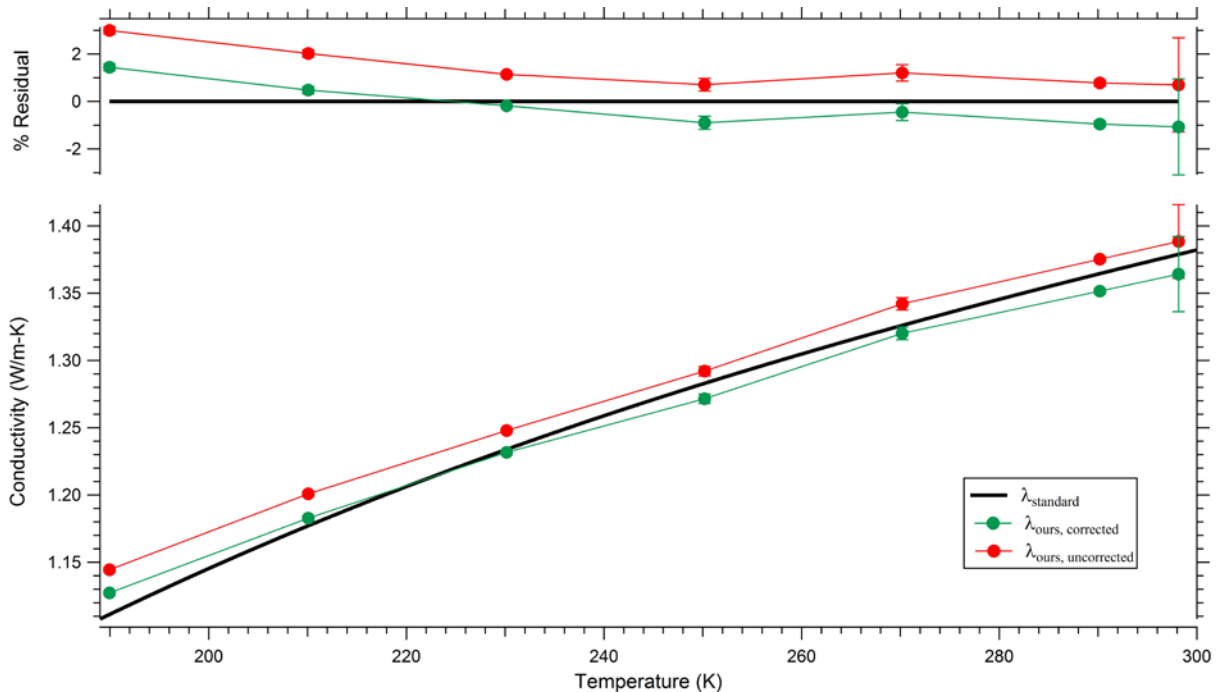


Figure 10: Fused Quartz Conductivity v Temperature. An NBS standard for fused quartz's conductivity (black) is overlaid with both the uncorrected (red) and zeroth-order-corrected (green) empirical data.

The corrected empirical conductivity falls within 2 percent of the NBS standard. While the accuracy is not bad in and of itself, its systematic tilt suggests the potential for improvement after

correcting to first-order. Fused quartz was chosen for apparatus calibration as its conductivity is on the order of ice's.

4.2 First-Order Conductivity Corrections

Applying Kirchhoff's circuit laws to the loops and nodes sketched in Fig. 5 results in the following set of equations:

$$\epsilon_B + I_3 R_3 + I_4 R_4 + I_5 R_6 = \epsilon_c \quad \text{Equation 9}$$

$$I_1 R_1 + I_2 R_2 + I_3 R_3 + I_4 R_4 + I_5 R_5 + I_6 R_6 + I_7 R_7 = I_8 R_8 + I_9 R_9 \quad \text{Equation 10}$$

With the exception of I_4 and I_5 (the current through the top and bottom halves of the sample, respectively), R_8 and R_9 (the contact resistances between the shield and the sample housing's base and copper cap, respectively) constitute the only unknowns. Pinning them down empirically should allow Eq. 8 and Eq. 9 to be solved simultaneously for I_4 and I_5 . The heat current lost through the sample's side should amount to the residual of the two currents.

4.3 Compliance Characterization

Figure 11 shows the results of several stainless steel presses after mounting the LVDT closer to the load cell.

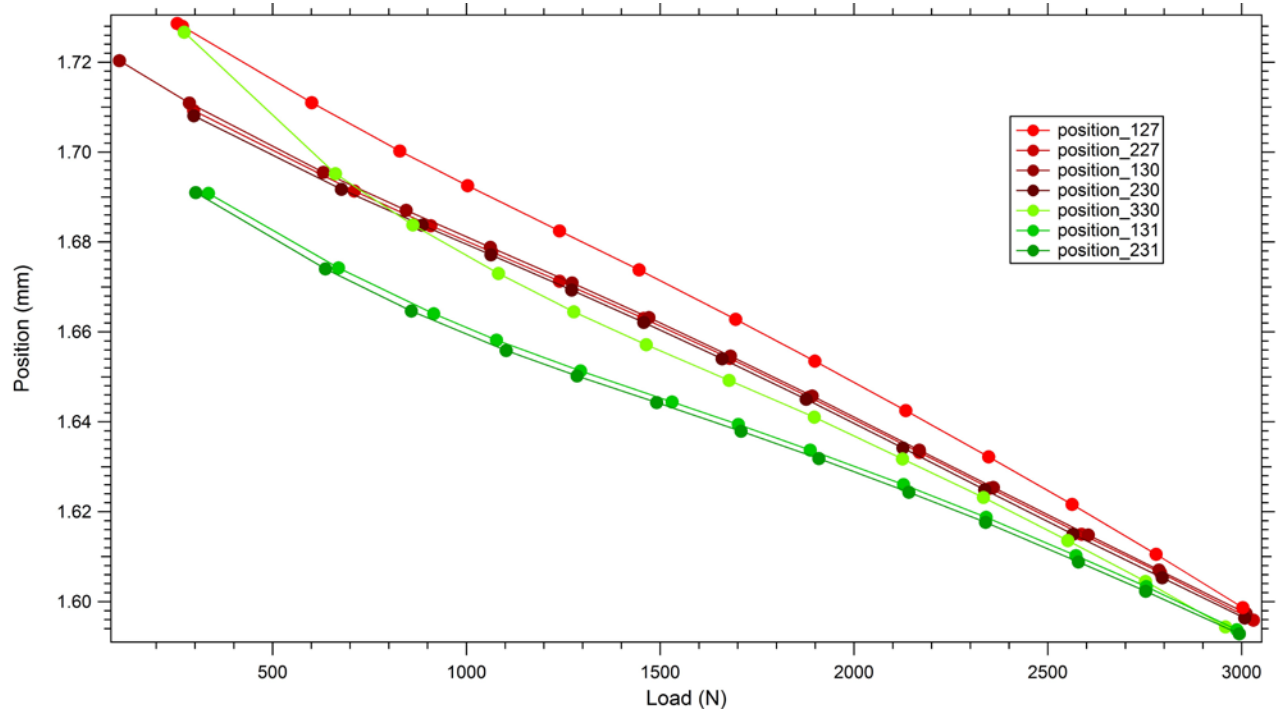


Figure 11: Total Displacement Measured by the LVDT v Applied Load, Corrected LVDT mounting. In the legend, each curve is labeled by the its trial number followed by the date of July the measurement was taken—i.e., 127 reads “the 1st trial on the 27th of July”.

The break between red and green symbolizes a complete apparatus remounting. Their tails of the two colors were brought together to eliminate the offset caused by remounting the LVDT shell.

Unfortunately, the curves irreproducibility trumps the resolution required for measuring sample compressions. Because the LVDT core is not designed to be loaded, removing the LVDT core from the load path is hypothesized to improve the compliance's reproducibility. A short-term remedy amounts to passing a titanium screw through the LVDT core's center and loading its end. Apparatus redesign is the long-term remedy.

4.4 Analog Preparation

The prepared water ice sample snapped while pressing it out of the ice press. Figure 12 shows a top-view of the salvaged sample.

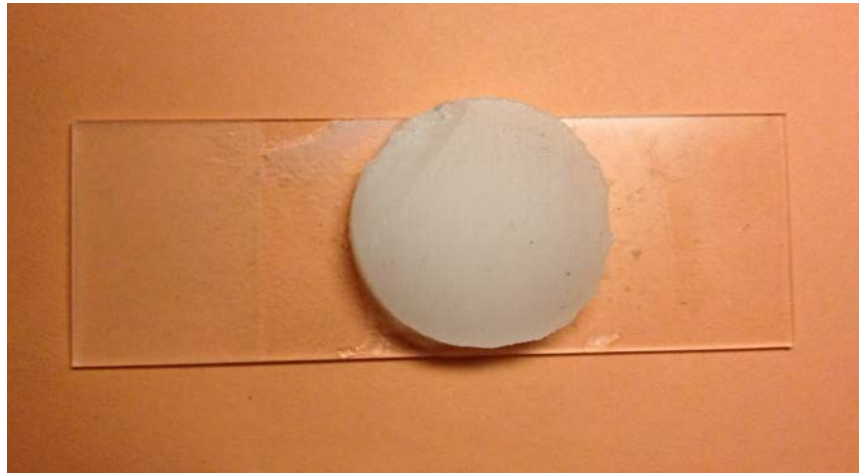


Figure 12: Top-view of the salvaged sample. Excepting the shear, it measures 0.23 inches thick and 1 inch in diameter.

The polycrystalline sample was prepared with grains between 200 and 300 microns.

Conclusion

Measuring the conductivity of fused quartz to within 2 percent of the accepted standard is an exciting accomplishment, but the systematic tilt of the residual suggests improvements may be found in accounting for heat loss through the sample's lateral face.

To do so, the validity in modeling the three-dimensional heat flow through the sample housing is being investigated. Thermal resistances of the sample housing's components as functions of temperature are actively being measured by strategically varying temperatures of the sample housing's platens, base, and shield.

While the response of the cryogenic apparatus to an applied load is presently irreproducible to the accuracy requisite for measuring sample compressions, altering the cryogenic apparatus' load path to avoid the LVDT core may improve results. It should be noted: measurements of the sample's compression as a function of applied load are insightful, but beyond this experiment's aim.

The snapped sample's conductivity will be measured as functions of temperature and stress, despite its irregular geometry. Hopefully doing so will yield empirical data indicative of the sample's creep rate.

Acknowledgement

This research was carried out at the Jet Propulsion Laboratory, California Institute of Technology, and was sponsored by JPL Summer Internship Program and the National Aeronautics and Space Administration.